Article

Molecular Cell

Calcium-Driven Folding of RTX Domain β-Rolls Ratchets Translocation of RTX Proteins through Type I Secretion Ducts

Graphical Abstract

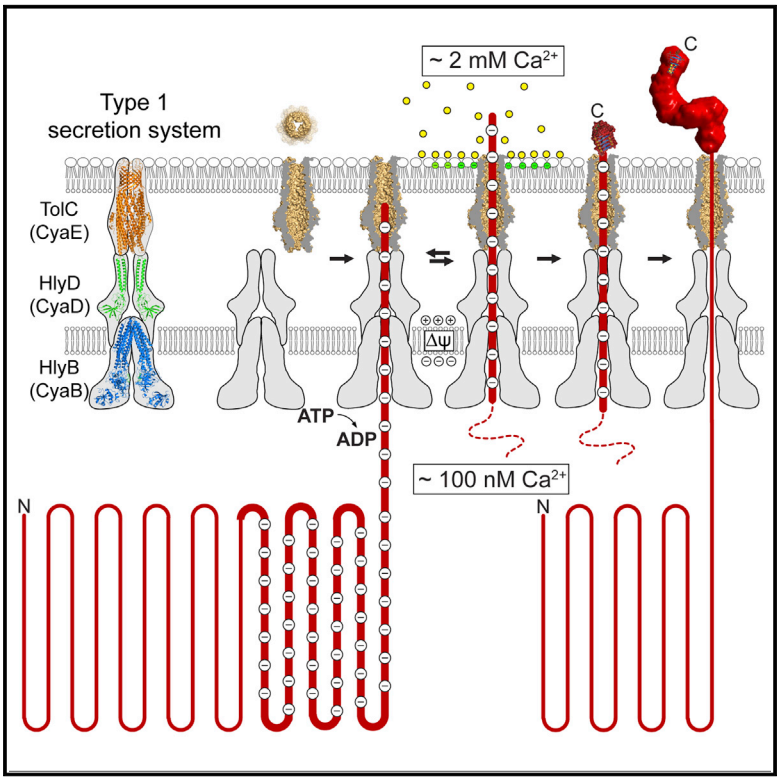

Authors

Ladislav Bumba, Jiri Masin, Pavel Macek, ..., Dmitri I. Svergun, Cyril Barinka, Peter Sebo

Correspondence

sebo@biomed.cas.cz

In Brief

Bumba et al. show that calcium-driven assembly of C-terminal capping structures triggers Ca^{2+}-dependent vectorial folding of RTX domains of leukotoxins. Successive formation of RTX β-roll structures then ratchets RTX protein translocation out of Gram-negative bacterial cells through the T1SS ducts.

Highlights

- Ca^{2+}-driven folding of C-terminal "capping structures" triggers folding of RTX proteins
- Vectorial folding of RTX domains proceeds successively from C toward N terminus
- Ca^{2+}-dependent RTX domain folding confers biological activity on RTX leukotoxins
- Ca^{2+}-driven folding of RTX β-rolls ratchets protein translocation through T1SS ducts

Accession Numbers

5CVW
5CXL

Bumba et al., 2016, Molecular Cell 62, 47–62
April 7, 2016 ©2016 Elsevier Inc.
http://dx.doi.org/10.1016/j.molcel.2016.03.018

Molecular Cell
Article

Calcium-Driven Folding of RTX Domain β-Rolls Ratchets Translocation of RTX Proteins through Type I Secretion Ducts

Ladislav Bumba,[1] Jiri Masin,[1] Pavel Macek,[1] Tomas Wald,[1] Lucia Motlova,[1,2] Ilona Bibova,[1] Nela Klimova,[1] Lucie Bednarova,[3] Vaclav Veverka,[3] Michael Kachala,[4] Dmitri I. Svergun,[4] Cyril Barinka,[5] and Peter Sebo[1,*]
[1]Institute of Microbiology, ASCR, v.v.i., Videnska 1083, 14220 Prague, Czech Republic
[2]Faculty of Science, Charles University in Prague, Vinicna 5, 128 44 Prague, Czech Republic
[3]Institute of Organic Chemistry and Biochemistry, ASCR, v.v.i., Flemingovo nam. 2, 16610 Prague, Czech Republic
[4]Hamburg Outstation, European Molecular Biology Laboratory, c/o DESY, Notkestrasse 85, D-22607 Hamburg, Germany
[5]Institute of Biotechnology, ASCR, v.v.i., Videnska 1083, 14220 Prague, Czech Republic
*Correspondence: sebo@biomed.cas.cz
http://dx.doi.org/10.1016/j.molcel.2016.03.018

SUMMARY

Calcium-binding RTX proteins are equipped with C-terminal secretion signals and translocate from the Ca^{2+}-depleted cytosol of Gram-negative bacteria directly into the Ca^{2+}-rich external milieu, passing through the "channel-tunnel" ducts of type I secretion systems (T1SSs). Using *Bordetella pertussis* adenylate cyclase toxin, we solved the structure of an essential C-terminal assembly that caps the RTX domains of RTX family leukotoxins. This is shown to scaffold directional Ca^{2+}-dependent folding of the carboxy-proximal RTX repeat blocks into β-rolls. The resulting intramolecular Brownian ratchets then prevent backsliding of translocating RTX proteins in the T1SS conduits and thereby accelerate excretion of very large RTX leukotoxins from bacterial cells by a vectorial "push-ratchet" mechanism. Successive Ca^{2+}-dependent and cosecretional acquisition of a functional RTX toxin structure in the course of T1SS-mediated translocation, through RTX domain folding from the C-terminal cap toward the N terminus, sets a paradigm that opens for design of virulence inhibitors of major pathogens.

INTRODUCTION

Secretion of proteins is central to bacterial interactions with the environment, and protein transport across the Gram-negative bacterial cell wall represents a particular challenge. Six dedicated pathways are employed by bacteria to excrete proteins across the sandwich of two biological membranes that enclose the peptidoglycan meshwork of bacterial sacculus (Costa et al., 2015). Of these type I (T1SS) to type VI (T6SS) secretion systems, the T2SS and T5SS operate by a two-step mechanism that involves periplasmic intermediates. The other four systems mediate a single-step translocation of exoproteins from cytosol of bacteria directly into the external milieu and even across a third membrane of a target cell (e.g., T3SS or T4SS).

T1SS is the least complex of these systems and is dedicated to excretion of the so-called repeats-in-toxin (RTX) family of exoproteins (Linhartová et al., 2010). These exhibit a broad array of biological activities and sizes (up to >8,000 residues) and share the presence of characteristic carboxy-proximal tandem repetitions of the Ca^{2+}-binding RTX nonapeptides of a consensual sequence GGxGxDxxx (Welch, 1991). The RTX repeats are organized into blocks that fold into a calcium-loaded structure known as the parallel β-roll (Baumann et al., 1993). The number of RTX repeat blocks per protein varies, and particularly vast RTX domains are found in the family of large T1SS-excreted RTX leukotoxins that play a major role in virulence of numerous Gram-negative pathogens (Linhartová et al., 2010; Satchell, 2011).

Pore-forming or multiple-activities-exhibiting RTX cytotoxins (MARTX) subvert host immunity by manipulation of phagocyte, lymphocyte, or epithelial cell functions. Among the best-studied RTX leukotoxins is the bifunctional adenylate cyclase toxin-hemolysin (CyaA, ACT, or AC-Hly) that plays a crucial role in host colonization by the human whooping cough agent *Bordetella pertussis* (Sebo et al., 2014; Vojtova et al., 2006). The RTX domain of CyaA consists of five RTX repeat blocks that bind extracellular calcium ions and fold into a structure that mediates toxin binding to the complement receptor 3 (CR3, known as Mac-1 or the $\alpha_M\beta_2$ integrin CD11b/CD18) on host phagocytes (Guermonprez et al., 2001). Upon binding to CR3, CyaA penetrates across the cytoplasmic membrane of phagocytes and translocates directly into their cytosol an adenylyl cyclase (AC) enzyme domain that binds intracellular calmodulin. This yields an extremely active AC enzyme that paralyzes cellular signaling and nearly instantaneously ablates the bactericidal functions of host phagocytes through unregulated conversion of cytosolic ATP into the key cellular signaling molecule cAMP. (Confer and Eaton, 1982; Eby et al., 2014; Kamanova et al., 2008).

The T1SS assemblies consist of three components, comprising an ABC (ATP-binding cassette) transporter incorporated as a polytopic protein into the inner bacterial membrane, a membrane fusion protein (MFP) extending from the inner membrane into periplasm, and a protein of the TolC family (OMP) that spans

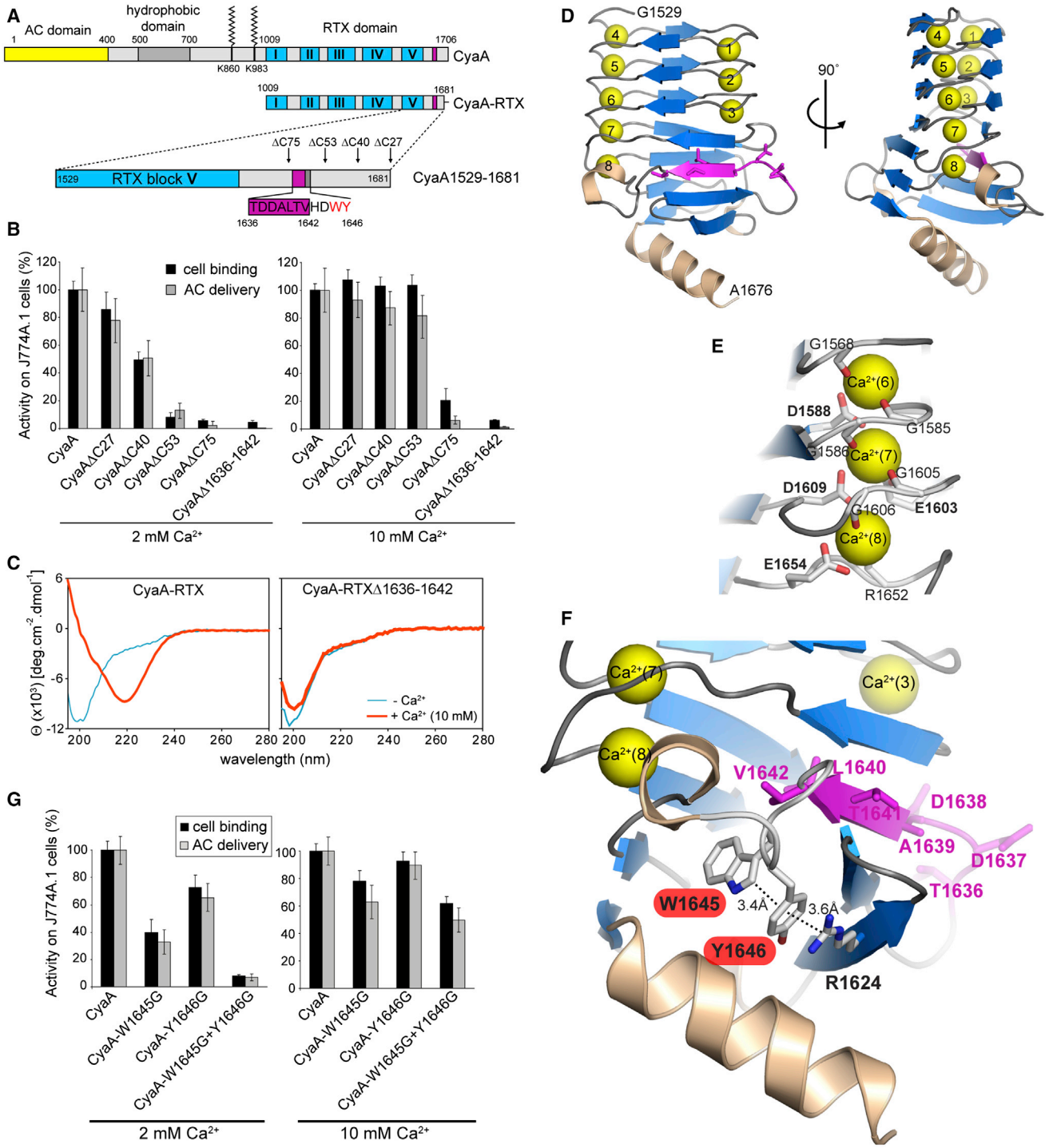

Figure 1. Assembly of a C-Terminal Capping Structure Triggers Ca^{2+}-Dependent Folding of the RTX Repeat Domain of CyaA

(A) CyaA consists of a cell-invasive AC enzyme that is fused to a C-terminal pore-forming RTX hemolysin moiety. The latter is covalently fatty acylated on Lys_{860} and Lys_{983} residues by CyaC, bears the C-terminal T1SS secretion signal, and comprises five RTX repeat blocks (I–V) formed by calcium-binding tandem repeats (GGxGxDxxx), respectively. Deletions within the $CyaA_{1529-1681}$ segment are indicated in the zoom out.

(B) Binding and cytotoxic activities of different CyaA constructs on mouse J774A.1 cells at 2 mM (left panel) or 10 mM Ca^{2+} concentrations (right panel). CyaA binding was assessed on J774A.1 cells exposed to 6 nM CyaA for 30 min at 4°C. AC domain delivery was assessed as accumulation of intracellular cAMP following incubation of cells with CyaA for 30 min at 37°C, as described in detail in Supplemental Experimental Procedures. The results represent average values of percent activity from four independent experiments. The error bars represent ± SD of the mean from at least three independent experiments performed in duplicates.

(legend continued on next page)

into periplasm from the outer membrane (Thomas et al., 2014b). The MFP hexamer connects the exit opening of the trimeric ABC transporter to the entry opening of the trimeric OMP conduit and seals the gated T1SS "channel-tunnel" assembly (Du et al., 2014), shielding the translocated polypeptides from periplasmic proteases. By difference to other protein translocation systems that recognize N-terminal secretion signals, the RTX protein substrates are targeted into and are led through the T1SS ducts by noncleavable C-terminal sequences (Lenders et al., 2015). Their interaction with the nucleotide binding domain (NBD) of the ABC transporter of T1SS triggers hydrolysis of ATP and provokes power strokes that enable insertion of the secreted protein into the T1SS conduit (Koronakis et al., 2000; Létoffé et al., 1996; Thanabalu et al., 1998). Both proton motive force across the inner bacterial membrane and the ATPase activity of the ABC transporter then appear to energize the early stages of T1SS translocation process (Koronakis et al., 1991). The mechanism underlying the directional translocation of the often very large RTX proteins (>>1,000 residues) through the T1SS duct remains, however, unclear.

We analyzed here the mechanism of T1SS-mediated secretion of CyaA from *B. pertussis* by assessing the structure and secretion kinetics of mutated CyaA. Postulating a paradigm of T1SS operation, we show that initiation of vectorial Ca^{2+}-driven folding of RTX repeats at their C terminus enables directional ratcheting of RTX protein translocation through T1SS ducts. This accelerates excretion and enables cosecretional folding of large RTX leukotoxins.

RESULTS

A Carboxy-Proximal Capping Assembly Is Essential for Ca^{2+}-Dependent Stacking of RTX Repeats into the β-Roll Structure and Acquisition of Leukotoxic Activity of CyaA

Previous work revealed that the C-terminal segment of CyaA (Figure 1A) is required for calcium-dependent folding of the last RTX repeat block and for cytototoxic activity of the T1SS-secreted CyaA toxin (Bauche et al., 2006; Bejerano et al., 1999; Chenal et al., 2010; Iwaki et al., 1995). Upon translocation through the T1SS conduit, this segment emerges on bacterial surface immediately after the C-terminal signal structure (Lenders et al., 2015), and its folding would provide the C-terminal entropic stabilization for folding of the last RTX repeat block of CyaA (Blenner et al., 2010). We hypothesized that folding of the C-terminal segment triggers calcium-dependent folding of the entire RTX domain of CyaA. We thus examined the capacity of the RTX domains of a set of C-terminally truncated toxins to adopt a functional fold. The proteins were purified under denaturing conditions in buffers containing 8 M urea, so as to mimic unfolding of the CyaA molecule during translocation through the T1SS conduit. The truncated RTX domains were then assessed for the capacity to fold in the presence of Ca^{2+} ions into a functional structure that would mediate CyaA binding to the CR3 and enable AC toxin penetration into macrophages (El-Azami-El-Idrissi et al., 2003). At physiological Ca^{2+} concentration (2 mM), these toxin activities were progressively lost with removal of the last 27, 40, 53, or 75 residues of CyaA (Figure 1B). However, the cell-binding activities of CyaAΔ_{C40} and CyaAΔ_{C53}, devoid of 40 or 53 C-terminal residues, were almost intact at 10 mM Ca^{2+}. Functional folding of the RTX domain could, hence, be enforced at 10 mM Ca^{2+} even when the 53 C-terminal residues were missing. In contrast, CyaA$\Delta_{C75,}$ or CyaA$\Delta_{1636\text{-}1642}$ lacking the TDDALTV heptapeptide (residues −63 to −71) recovered little or no activity in 10 mM Ca^{2+}. Folding capacity of the RTX domain of CyaA$\Delta_{1636\text{-}1642}$ was thus examined by circular dichroism (CD) spectroscopy (Figure 1C). A prominent negative peak at 217 nm, corresponding to formation of the β-roll structures (Chenal et al., 2010), was indeed observed for the complete purified CyaA-RTX domain (residues 1,009 to 1,681 of CyaA), which underwent a characteristic Ca^{2+}-induced transition from the intrinsically disordered to the folded state already at 2 mM Ca^{2+}. In contrast, no formation of β roll in CyaA-RTX$\Delta_{1636\text{-}1642}$ was detected even at 10 mM Ca^{2+}. The C-terminal residues −53 and −75, hence, comprise at least part of the segment that is essential for Ca^{2+}-dependent folding of the RTX domain.

To gain more insight, we solved the X-ray structure of the CyaA$_{1529\text{-}1681}$ fragment comprising the last RTX repeat block (block V) and the segment required for Ca^{2+}-dependent folding. Diffracting crystals were obtained in orthorhombic (I222) and tetragonal ($P4_12_12$) space groups, with one or two monomer subunits per asymmetric unit (Figure S1, available online), yielding near identical independent structures at 1.25 Å (I222) and 1.45 Å ($P4_12_12$) resolution (Tables 1 and S1).

CyaA$_{1529\text{-}1681}$ adopts a "hatchet head"-like structure with an N-terminal "blade"-like β-roll that progressively broadens into a "hammerhead" capping structure formed by the C-terminal residues (Figure 1D). The β-roll within residues 1,529–1,613 comprises nine GGxGxDxxx motif-like nonapeptides arranged regularly within a right-handed parallel β helix. Seven out of the eight

(C) Far-UV CD spectra of CyaA-RTX (left panel) and CyaA-RTX$\Delta_{1636\text{-}1642}$ (right panel) in the absence (blue line) and in the presence of 10 mM $CaCl_2$ (red line).
(D) X-ray structure of CyaA$_{1529\text{-}1681}$. The N-terminal consecutive nonapeptide tandem repeats (GGxGxDxxx) are arranged in a regular right-handed helix of parallel β strands (β-roll). The first six residues of the RTX motif (GGxGxD) constitute a turn with bound calcium ion (yellow ball), while the last three nonconserved residues (xxx) form a short β strand. Calcium ions are numbered for clarity, and the residues 1,636–1,642 of the TDDALTV segment involved in initiation of Ca^{2+}-induced folding of the RTX domain are colored in magenta.
(E) Close-up view of calcium-binding sites within the C-terminal segment of CyaA$_{1529\text{-}1681}$. Ca^{2+}(6) and Ca^{2+}(7) are completely buried within the turns and are regularly coordinated by the side chains of Asp residues in position 6 (Asp_{1588} and Asp_{1609}) and backbone carbonyl groups of Gly residues of the GGxGx**D**xxx motif, respectively. Ca^{2+}(8) is more exposed to the solvent and is coordinated by side chains of Asp_{1609} and Glu_{1654} along with backbone carbonyls of Gly_{1606} and Arg_{1652} and two water molecules (data not shown). The carbon and oxygen atoms are represented in gray and red color, respectively.
(F) Detailed view of the C-terminal capping structure of the CyaA$_{1529\text{-}1681}$ segment. The TDDALTV heptapeptide is highlighted in magenta. The indole ring of Trp_{1645} is positioned perpendicularly to the benzene ring of Tyr_{1646}, which itself interacts with the positively charged guanidinium group of Arg_{1624} in a cation-π-π interaction.
(G) CR3-binding and cell-invasive activity of CyaA constructs with glycine substitutions of the Trp_{1645} and Tyr_{1646} residues. The error bars represent ± SD of the mean from at least three independent experiments performed in duplicates.

Table 1. X-Ray Data Collection and Refinement Statistics

	$CyaA_{1529-1681}$ (5CVW)	$CyaA_{1529-1681}$ (5CXL)
Data Collection		
Space group	Orthorhombic I222 (23)	Tetragonal $P4_12_12$ (92)
Wavelength (Å)	0.9181	0.9181
Cell dimensions		
a, *b*, *c* (Å)	62.8, 62.9, 77.6	52.2, 52.2, 195.9
α, β, γ (°)	90, 90, 90	90, 90, 90
Resolution (Å)	29.24–1.23 (1.30–1.23)	50–1.45 (1.54–1.45)
R_{sym} or R_{merge}	4.3% (54.5%)	5.2% (74.1%)
$I / \sigma(I)$	19.78 (2.48)	22.11 (2.55)
Completeness (%)	93.6 (72.3)	99.9 (99.8)
Redundancy	4.48	8.59
Refinement		
Resolution (Å)	29.24–1.25 (1.28–1.25)	32.15–1.45 (1.49–1.45)
Number of reflections	39,012 (2,217)	46,709 (3,344)
R_{work}	0.147 (0.206)	0.152 (0.188)
R_{free}	0.180 (0.272)	0.208 (0.270)
Number of atoms	1,263	2,417
Protein	1,107	2,172
Ligand/ion	32	24
Water	124	221
β factors (overall)	16.0	22.6
Protein	14.5	21.6
Ligand/ion	21.6	20.8
Water	29.5	32.8
Rmsds		
Bond lengths (Å)	0.017	0.019
Bond angles (°)	1.95	1.92
Ramachandran plot[a]		
Favored regions (%)	97.3	95.21
Additionally allowed (%)	2.7	4.47
Outliers (%)	0	0.32

[a]Calculated with MolProbity (Chen et al., 2010).

predicted Ca^{2+}-binding sites within the β-roll turns, on both sides of the β-roll, contain completely buried Ca^{2+} ions. These are periodically coordinated by carboxyl groups of the side chains of aspartic acids at position 6 and by carbonyl groups of the polypeptide backbone at positions 1–5 of the GGxGx**D**xxx motif. An exception is the carboxy-proximal $Ca^{2+}(7)$, where the backbone carbonyl group at position 1 of the nonapeptide motif is replaced by the side chain of Glu_{1603} residue (Figure 1E). By difference to the seven Ca^{2+} ions buried within the β-roll, the $Ca^{2+}(8)$ ion is more accessible to solvent and uses two water molecules as ligands. It is coordinated by the side chain carboxyls of Asp_{1609} and Glu_{1654} and the backbone carbonyls of Gly_{1606} (from the last turn of the β-roll) and Arg_{1652}. This explains why the $CyaA_{\Delta C53}$ protein exhibits only a residual (~10%) receptor-binding capacity of the RTX domain at 2 mM Ca^{2+} (cf. Figure 1B), as absence of Glu_{1654} would reduce the affinity of the $Ca^{2+}(8)$ binding site. Its loading would, hence, occur and provide stabilization of the fold only at supraphysiological Ca^{2+} concentration (e.g., 10 mM).

The structure formed by residues 1,614–1,676 caps the β-roll by an assembly of antiparallel β strands (two and three extending the β-roll on each side) with a short amphipatic α helix at the tip (Figure 1F). The highly hydrophobic interior of the capping structure communicates with the hydrophobic interior of the β-roll, and the entire capping assembly would form a scaffold on which the β-roll stack of RTX block V can assemble upon exit from the T1SS duct. The $_{1639}ALTV_{1642}$ segment of the TDDALTV heptapeptide forms a short β strand parallel to the adjacent β strand of the RTX β-roll. The contiguity of the β-roll with the antiparallel β strand assembly makes the two surfaces of the $CyaA_{1529-1681}$ structure, consisting of five parallel and two or three antiparallel β sheets, respectively. Despite little sequence conservation, similar structures are conserved also in the C-terminal portions of T1SS-secreted RTX lipases and proteases (Figure S1).

The Asp_{1637} and Asp_{1638} residues of the TDDALTV segment and the Asp_{1644}, Asp_{1648}, and Asp_{1650} residues are not involved in binding of calcium ions. Their alanine or valine substitutions had, indeed, little impact on functional folding of the CyaA-RTX domain (data not shown). Within this highly negatively charged segment, however, there are two aromatic Trp_{1645} and Tyr_{1646} residues that are conserved in the C-terminal segments of RTX leukotoxins (see Figure 4). The indole ring of Trp_{1645} is inserted deep into the hydrophobic core of the C-terminal capping structure and is positioned perpendicularly to the benzene ring of Tyr_{1646} (Figure 1F), lying parallel to the side chain of Arg_{1624} from an antiparallel β strand of the capping structure. The spatial arrangement and distances (3.4 Å and 3.6 Å) would enable a cation-π-π interaction between the positively charged guanidinium group of Arg_{1624} and the aromatic benzene and indole rings of Tyr_{1646} and Trp_{1645} (Figure 1F). This appears to play a central role in formation of the hydrophobic core and folding of the capping structure upon exposure to Ca^{2+} (Figure 1G). Glycine substitutions of Tyr_{1646} (W1645G) or Trp_{1645} (Y1646G) provoked, indeed, a partial loss of RTX domain function (cell binding) at 2 mM Ca^{2+}. The W1645G + Y1646G combination then had a highly synergic effect, decreasing ~10-fold the capacity of $CyaA_{W1645G+Y1646G}$ to bind the CR3 receptor at 2 mM Ca^{2+}. Functional folding of the RTX domain of $CyaA_{W1645G+Y1646G}$ could, however, still be enforced at 10 mM Ca^{2+} (Figure 1G; see also Ca^{2+} titration in Figure 2). This suggests that positioning of side chain carboxyls of Asp_{1609} and Glu_{1654} and of backbone carbonyls of Gly_{1606} and Arg_{1652} would enable formation and loading of the $Ca^{2+}(8)$ ion binding site. The ensuing structural stabilization would then enable a cation-π-π interaction of side chains of the Trp_{1645}, Tyr_{1646}, and Arg_{1624} residues. Due to reduction of folding space, the entire capping structure would next fold.

Calcium-Dependent Folding of the T1SS-Excreted Leukotoxin CyaA Is Initiated at a Carboxy-Proximal β-Roll Capping Structure and Proceeds Sequentially toward the N Terminus of the RTX Domain

To analyze the Ca^{2+}-dependent folding pathway of the C-terminal β-roll domain, titration of the $CyaA_{1529-1681}$ fragment with

Ca^{2+} was followed by far-UV CD spectroscopy. Transition of $CyaA_{1529-1681}$ from an intrinsically disordered state into the folded β-roll occurred as a two-stage process, triggered at 0.2 mM Ca^{2+} and completed at <2 mM Ca^{2+} (Figure 2A). Similar Ca^{2+} dependence of folding was observed also for the homologous $HlyA_{733-975}$ segment of *E. coli* α-hemolysin (HlyA), showing that Ca^{2+}-driven folding of RTX leukotoxins involves a two-stage mechanism (Figure S2).

To decipher the folding pathway in a residue-specific manner, Ca^{2+}-induced conformational changes of ^{15}N-labeled $CyaA_{1529-1681}$ were followed by NMR spectroscopy. In the absence of Ca^{2+}, the ^{1}H-^{15}N HSQC spectrum of the $CyaA_{1529-1681}$ yielded a characteristic narrow dispersion of amide resonances of a disordered protein that lacks regular conformation (Figure 2B). Upon exposure to Ca^{2+}, these HSQC crosspeaks were replaced by distinct and well-dispersed resonances characteristic of folded proteins. Individual ^{1}H-^{15}N crosspeaks were unambiguously assigned to backbone amides at coverage of 89% for the calcium-free and 71% for the calcium-loaded $CyaA_{1529-1681}$ polypeptide, respectively (Figure S3). Analysis of chemical shifts revealed that in the absence of Ca^{2+}, the secondary structure formation propensities of individual residues were very low, revealing absence of regular structural elements in the apo form. In contrast, the secondary structure propensities in the Ca^{2+}-loaded $CyaA_{1529-1681}$ revealed a series of short β strands and a C-terminal α helix (Figure S3; cf. X-ray structure in Figure 1D).

As $CyaA_{1529-1681}$ protein concentrations in the NMR experiments (~1 mM) were in the range of K_d for Ca^{2+} (0.4–1.5 mM), a quantitative equilibrium titration of $CyaA_{1529-1681}$ at distinct Ca^{2+}-to-protein ratios (CPRs) was performed. The increase in relative intensity of the peaks was then used to monitor the Ca^{2+}-dependent folding pathways of individual residues. The C-terminal part of the $CyaA_{1529-1681}$ began to fold at a CPR of 2 to 3, as exemplified by the green-colored crosspeaks in the zoomed-out sections of the HSQC spectra (Figure 2C), and by the corresponding green titration curves of Gly_{1597} and Asp_{1638} (Figure 2D). As documented by the full HSQC spectra and titration curves of the well-resolved crosspeaks (Figure S4), the residues involved in formation of the C-terminal capping structure were reaching the final folded position already at CPR of 2 to 4. The N^{ε}-H^{ε} group of the indole ring of Trp_{1645} reached its final position at CPR of 3 to 4 (Figure 2D), indicating an early completion of assembly of the capping structure. Formation of the β-roll assembly proceeded in a cooperative manner, and binding of each additional Ca^{2+} ion enhanced the "cooperativeness" of Ca^{2+} loading and folding, increasing gradually from the C toward the N terminus (Figures 2D and S4). The residues of the central portion of the β-roll (orange peaks and curves) started to fold at CPR of 3 to 5, and the N-terminal portion (red residue peaks and curves) remained unfolded until a CPR of 4 to 6, at which Ca^{2+} binding triggered folding of the Gly_{1557} and Ser_{1555} backbone amides (Figure 2D). A ratio of eight to nine Ca^{2+} ions per protein molecule was required for full loading and folding of $CyaA_{1529-1681}$. This goes well with the number of eight Ca^{2+} ions resolved in the X-ray structure of $CyaA_{1529-1681}$ (cf. Figure 1D).

The double substitution of Trp_{1645} and Tyr_{1646} by glycines importantly affected the Ca^{2+}-dependent folding of $CyaA_{1529-1681}$ (Figure 2A). $CyaA_{1529-1681}/_{W1645G+Y1649G}$ started to fold at higher than 1 mM Ca^{2+} or a CPR ratio of 4, with complete folding occurring only at 10 mM Ca^{2+} (Figures 2E, 2F, and S5). The highly cooperative CPR-folding function reflected a single-stage process triggered at about 10-fold higher Ca^{2+} concentrations than folding of intact $CyaA_{1529-1681}$ (cf. Figure 2A), documenting the essential role of Trp_{1645} and Tyr_{1646} in the nucleation of capping structure assembly.

X-ray crystallography data and NMR titrations allowed delineation of the folding pathway of the C-terminal part of CyaA as a highly cooperative process that proceeded in a strictly sequential manner from the C terminus toward the N terminus (Figure 2G). Formation of the first calcium binding site [Ca^{2+}(8)] appears to be accompanied by assembly of a bundle of three antiparallel β strands between residues Leu_{1620} and Val_{1643}. Hydrophobic interactions with the β strands on the opposite face of the β barrel (residues 1,655–1,658 and 1,609–1,613) would then lead to formation of a hydrophobic core of the capping structure (green) and sequential stacking of RTX β strands into the β-roll of a regular right-handed parallel β helix (orange and red). Structural similarity within the C-terminal parts of other RTX domains suggests that this would represent a general folding pathway of the β-roll domains of RTX proteins (cf. Figure S1).

Low-resolution structure of the entire CyaA-RTX domain ($CyaA_{1009-1681}$) by small-angle X-ray scattering (SAXS) in solution revealed that the entire folded RTX domain of CyaA is an elongated molecule that consists of five tightly packed segments (Figure 3; Table S2). Superimposition of the solved 3D structure of $CyaA_{1529-1681}$ (cf. Figure 1D) onto the low-resolution model of the RTX domain built from the SAXS data revealed that the size and shape of $CyaA_{1529-1681}$ corresponds to a distinct β-roll segment at the tip of the RTX domain. It is plausible to assume that each of the five discernible segments in the SAXS structure corresponds to a single RTX repeat block folded into a β-roll structure, in good agreement with the recently proposed RTX domain models (O'Brien et al., 2015).

Similar C-Terminal Folding-Nucleating Capping Structures Are Required for Calcium-Dependent Folding and Biological Activities of Other RTX Leukotoxins

We next examined the C-terminal segments of several other RTX leukotoxins for the presence of structures homologous to the capping structure of CyaA. Multiple sequence alignment revealed that such segments were located between the conserved RTX motifs (GGxGxDxxx) and the secretion signals of *E. coli* HlyA, LtxA leukotoxin of *A. actinomycetemcomitans*, and ApxIA hemolysin of *A. pleuropneumoniae* (Figure 4A). These sequences exhibited a consensus motif $_{*}$T$_{*}$+XWF (Figure 4B), forming the central part of the $CyaA_{1636-1650}$ sequence, where $_{*}$ stands for an aliphatic amino acid, and + represents a positively charged residue. Deletion of homologous segments in the other leukotoxins yielded $HlyA\Delta_{905-919}$, $ApxIA\Delta_{902-916}$, and $LtxA\Delta_{892-906}$ proteins that were unable to lyze sheep erythrocytes or Jurkat T cells, respectively (Figures 4C–4E, upper panels). As further determined by CD spectroscopy, the loss of biological activity correlated with the loss of capacity of the respective purified

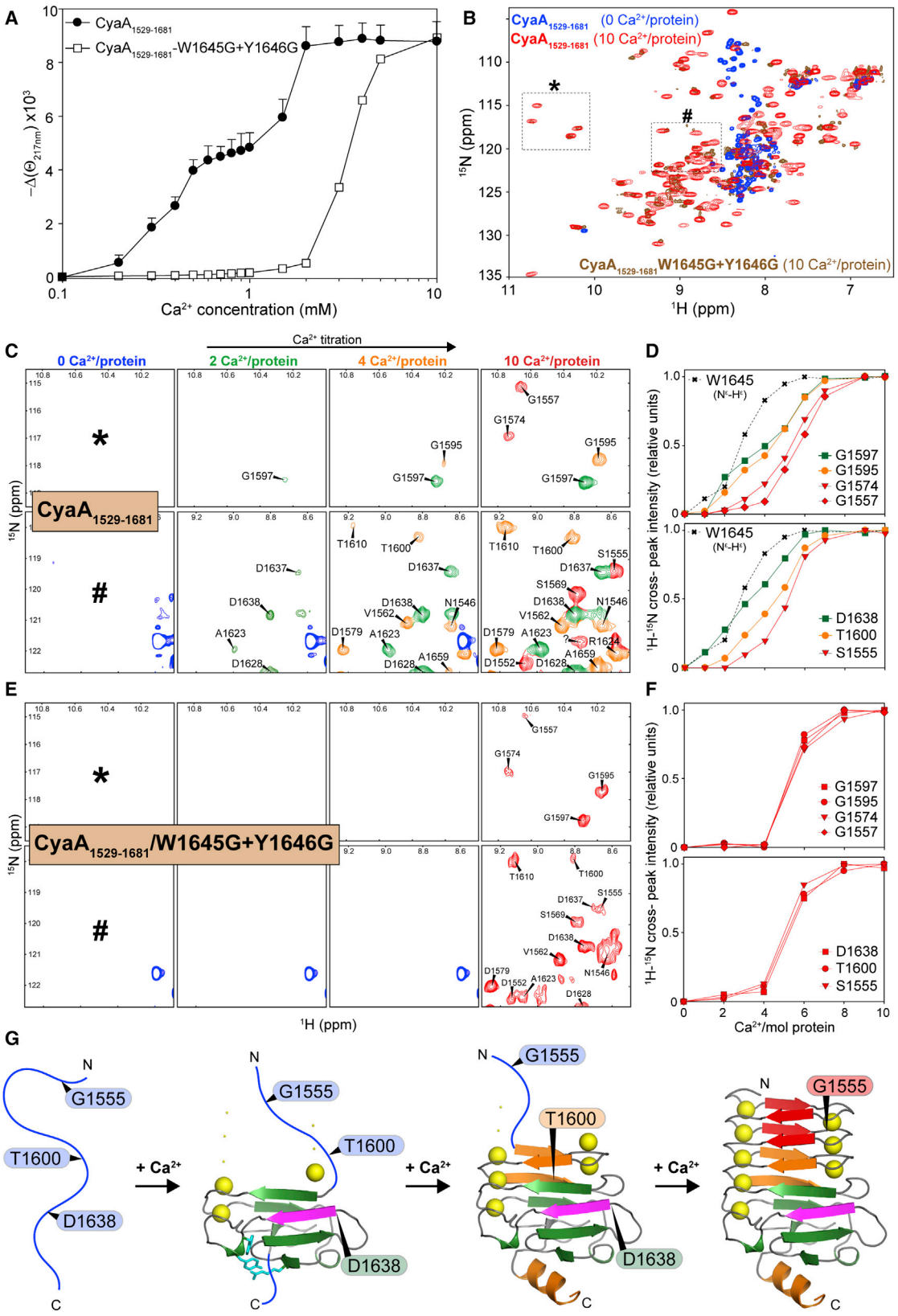

(legend on next page)

HlyA-RTXΔ$_{905-919}$, ApxIA-RTXΔ$_{902-916}$, and LtxA-RTXΔ$_{892-906}$ domains to undergo Ca^{2+}-dependent folding into the parallel β-roll structures (Figures 4C–4E, lower panels). Similar C-terminal capping structures as that found in CyaA, hence, play a central role in Ca^{2+}-dependent folding of several RTX leukotoxins.

Biological Activity of CyaA in *B. pertussis* Infections Depends on the Integrity of the C-Terminal β-Roll Capping Structure

To relate the in vitro data to folding requirements during in vivo secretion of CyaA, we introduced the mutations disrupting the β-roll capping structure into the *cyaA* gene on *B. pertussis* chromosome and examined the virulence of the mutant strains in mice. Intranasal administration of 1.5×10^8 CFU (colony-forming units) of wild-type *B. pertussis* provoked death of all inoculated mice within 2 days (Figure 5). However, up to 60% of mice survived the challenge for 4 days with a 10-fold increased dose of 1.5×10^9 CFU of the mutant producing CyaA$_{W1645G+Y1646G}$, which exhibits a residual (~10%) binding and toxin activity at 2 mM Ca^{2+} (physiological) and folds only at 10 mM Ca^{2+} (cf. Figure 1G). No lethality was then observed even at a 100-fold increased inoculum dose of the mutant secreting CyaAΔ$_{1636-1642}$ that is unable to fold even at 10 mM Ca^{2+} and is inactive as toxin (cf. Figures 1B and 1C). The LD_{50} values were then approximately ten times higher for the CyaA$_{W1645G+Y1646G}$-secreting mutant (1.5×10^9 CFU) than for the wild-type bacteria (1×10^8 CFU). This goes well with the ~10-fold reduced in vitro specific toxin activity of the purified CyaA$_{W1645G+Y1646G}$. The capacity of the RTX domain to fold in the presence of Ca^{2+} and mediate phagocyte binding of CyaA was thus crucial for *B. pertussis* virulence.

Ca^{2+}-Binding-Promoted Cosecretional Folding of the RTX β-Rolls Generates Brownian Molecular Ratchets that Accelerate Protein Excretion through T1SS

Translocation of RTX proteins through T1SS conduits is led by the C-terminal signal segments (Lenders et al., 2015). Therefore, we tested the hypothesis that protein secretion through T1SS is facilitated by vectorial Ca^{2+}-dependent folding of the RTX repeats, as they emerge from the opening of the T1SS conduits. Efficacy of secretion of CyaA and of its folding-deficient CyaAΔ$_{1636-1642}$ variant was compared in culture media containing 0.1 mM or 2 mM Ca^{2+} concentrations that prevent or promote folding of the RTX domain of CyaA, respectively (cf. Figure 1). At both Ca^{2+} concentrations, the two *B. pertussis* strains grew with the same rate (Figure S6). Advantage was further taken of the very high specific AC enzyme activity of CyaA complexes with calmodulin. This enabled reliable quantitation of CyaA distribution between culture supernatant, cell-associated, and intracellular fractions (Sebo and Ladant, 1993) thanks to the capacity of the AC enzyme domain to refold independently of the rest of the CyaA molecule, with the AC enzyme quantitatively recovering its activity when diluted out from 8 or 4 M urea extracts into the AC assay buffer containing calmodulin (Karst et al., 2010).

B. pertussis is typically grown in vitro in liquid media with Ca^{2+} concentrations as low as 0.1 mM (Stainer and Scholte, 1970). Under such conditions, the majority of excreted CyaA molecules remains adsorbed to the outer surface of *B. pertussis* cells (Zaretzky et al., 2002). Such presumably unfolded CyaA molecules can, however, be quantitatively desorbed from the surface of unbroken cells into 4 M urea solution (Hewlett et al., 1989). We thus determined the total amount of secreted CyaA (AC_{out}) as the sum of the surface-associated AC enzyme desorbed into 4 M urea plus the amount of AC enzyme recovered in culture supernatants. The intracellular CyaA was then quantitated as the AC activity (AC_{in}) recovered in extracts of cells solubilized in 8 M urea once the surface-associated CyaA has been stripped off with 4 M urea, thus allowing quantitation of CyaA in supernatants and subcellular fractions (Sebo and Ladant, 1993).

At 0.1 mM Ca^{2+}, at which the RTX domain does not fold, the wild-type (*Bp*) and mutant (*Bp*-CyaAΔ$_{1636-1642}$) strains produced comparable total amounts of CyaA (Figure 6B, upper panel). Both proteins were, hence, secreted with an equal background efficacy (AC_{out}/AC_{in} ~1), where ~50% of the produced toxin molecules remained intracellular (Figure 6B, lower panel, red bar) and ~50% reached cell surface and/or were released into the medium (Figure 6B; sum of red, green, and black bars from the lower panel plotted as a black bar in the central panel). Hence, the capacity of the C-terminal secretion signal to engage the T1SS apparatus and direct translocation across the cell envelope was not compromised in CyaAΔ$_{1636-1642}$. An important difference in secretion efficacy of the two proteins was, however, observed when the bacteria were grown in media containing 2 mM Ca^{2+}, promoting RTX domain folding. The total produced

Figure 2. Vectorial Ca^{2+}-Dependent Folding Starts at the C Terminus and Proceeds Sequentially toward the N Terminus of the RTX Block V of CyaA

(A) Ca^{2+}-dependent folding of the C-terminal RTX block V and capping structure segments of CyaA$_{1529-1681}$ and CyaA$_{1529-1681/W1645G+Y1646G}$. The proteins (100 μg/ml) were titrated with Ca^{2+}, and molar ellipticity change at 217 nm [$-\Delta(\Theta_{217\ nm})$] was measured. The error bars represent ± SD of the mean from three independent experiments.

(B) Overlay of the ^1H-^{15}N HSQC spectra of 1 mM ^{15}N-labeled CyaA$_{1529-1681}$ in the presence (red) or absence (blue) of 10 mM Ca^{2+} and of the spectra of 1 mM ^{15}N-labeled CyaA$_{1529-1681/W1645G+Y1646G}$ at 10 mM Ca^{2+} (orange).

(C and E) Close-up views of two selected sections of well-resolved ^1H-^{15}N HSQC spectra from titration of CyaA$_{1529-1681}$ and CyaA$_{1529-1681/W1645G+Y1646G}$ with Ca^{2+}. The peaks from within each spectrum were separated and colored differently according to their order of appearance in the titration, so as to reflect the sequence of appearance of crosspeaks of individual backbone amides at their final positions in the fold, in function of the CPR: blue, unfolded state at CPR = 0; green, folding at CPR = 2; orange, folding at CPR = 4; red, folding at CPR = 10, respectively.

(D and F) Ca^{2+}-dependent folding pathways of backbone amides of selected residues. Relative intensities of selected residue crosspeaks from 2-D ^1H-^{15}N HSQC spectra of Ca^{2+}-titrated CyaA$_{1529-1681}$ and CyaA$_{1529-1681/W1645G+Y1646G}$ at indicated CPRs. Maximal intensity of each individual crosspeak was set to 1.

(G) The model of Ca^{2+}-induced sequential folding of CyaA$_{1529-1681}$. In the absence of Ca^{2+}, CyaA$_{1529-1681}$ remains unfolded (blue). Upon binding of the first two to three Ca^{2+} ions, the C-terminal capping structure (green) is formed (the ALTV β strand is in magenta) and serves as folding scaffold for stacking of the RTX repeats into the β-roll fold (orange and red). See (C) for color codes of residue folding into final position.

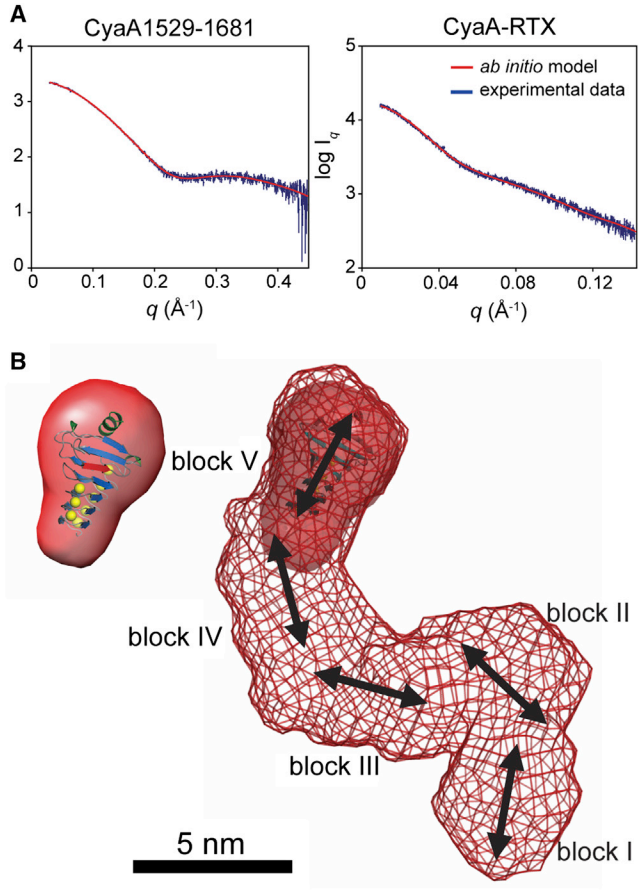

Figure 3. The Low-Resolution 3D Model of the Folded RTX Domain of CyaA

(A) SAXS plots of $CyaA_{1529-1681}$ (left panel) and CyaA-RTX (right panel) in the presence of 10 mM Ca^{2+}. Experimental curves are shown as blue dots with error bars, and the theoretical scattering intensities derived from the ab initio models are given as continuous red lines. The intensity is displayed as a function of momentum transfer q.

(B) Superposition of the X-ray structure of $CyaA_{1529-1681}$ (PDB ID 5CVW) with the surface envelope obtained from the SAXS data (left panel), overlaid on the ab initio model of the entire RTX domain of CyaA (CyaA-RTX, meshed envelope). The putative location of individual RTX block of CyaA (I–V) is indicated by black double-sided arrows.

amounts of the two proteins did not change (Figure 6B, upper panel), but only ~5% of the folding-competent CyaA remained intracellular (Figure 6B, lower panel, red bar), ~95% of the produced CyaA was secreted at 2 mM Ca^{2+} (Figure 6B, central panel), and ~90% of total produced CyaA was released from cell surface into culture supernatant (Figure 6B, lower panel, black bar). Presence of 2 mM Ca^{2+} thus resulted in a strong (>20-fold) increase of the efficacy of CyaA secretion, yielding an AC_{out}/AC_{in} ratio of ~24. In contrast, secretion of the folding-deficient $CyaA\Delta_{1636-1642}$ was less enhanced in the presence of 2 mM Ca^{2+}, with >20% of the $CyaA\Delta_{1636-1642}$ molecules remaining intracellular and the amount of secreted protein being enhanced by a factor of only ~1.3, raising the AC_{out}/AC_{in} ratio to ~4, with ~40% of the translocated $CyaA\Delta_{1636-1642}$ molecules remaining attached to cell surface (Figure 6B, lower panel, green bar). In line with that, the rate of secretion of $CyaA\Delta_{1636-1642}$ in media with 2 mM Ca^{2+} was 1.8 ± 1.0 pmol.min^{-1}, while a two-times-higher secretion rate of 3.6 ± 1.4 pmol.min^{-1} was found for intact CyaA (Figure 6C). Hence, the Ca^{2+}-dependent folding of RTX repeats accelerated the translocation of CyaA molecules through the T1SS conduits and prevented adsorption and accumulation of unfolded secreted CyaA on bacterial surface.

Intriguingly, ~50% of CyaA molecules still accomplished translocation to bacterial surface through T1SS even when external Ca^{2+} concentration was too low to promote RTX folding. Hence, upon engagement of the inner membrane ATPase, the translocation through the T1SS duct proceeded, and it was accelerated, but not driven, by Ca^{2+}-driven folding of the exiting RTX domain. To examine if the multiple RTX repeat blocks play a folding-independent role in CyaA secretion, we assessed the secretion efficacy of $CyaA\Delta_{RTX\_I-IV}$ protein that has the first four RTX repeat blocks (I–IV) deleted (Figure 6A), while having the RTX block V with the capping structure and secretion signal intact. Despite comparable mRNA transcript levels (Figure S6), $CyaA\Delta_{RTX\_I-IV}$ was produced in substantially lower amounts than intact CyaA (Figure 6B, upper panel), indicating degradation of nonsecreted $CyaA\Delta_{RTX\_I-IV}$ inside cells. $CyaA\Delta_{RTX\_I-IV}$ secretion was, indeed, inefficient ($AC_{out}/AC_{in} \leq 0.15$) even at 2 mM Ca^{2+}, and >85% of the $CyaA\Delta_{RTX\_I-IV}$ molecules remained intracellular (Figure 6B, lower panel). Efficient translocation of the 1,008 residue-long N-terminal portion of CyaA through the T1SS duct, hence, required more than the presence and folding of RTX block V.

The number of RTX repeats contained in the RTX domains of the annotated RTX proteins correlates to some extent with the size of the non-RTX portions of the respective T1SS-translocated protein (Figure S7). We thus hypothesized that the overall negative charge of the RTX domain might facilitate its electrophoretic extrusion from bacterial cytosol through the T1SS conduit, along the gradient of negative potential on the inner bacterial membrane. To test this, the net negative charge of the C-terminal RTX block V of CyaA was reduced by 11 charge-reversing lysine and arginine substitutions, replacing the negatively charged residues that are not directly involved in binding of Ca^{2+} ions. This increased the theoretical isoelectric point of RTX block V from pI (isoelectric point) of 3.7 to pI 6.6 and resulted in a reduced efficacy of the T1SS-mediated secretion of $CyaA_{9D2E/9K2R}$ (Figure 6B). Over 60% of the $CyaA_{9D2E/9K2R}$ molecules remained cytosolic, and the efficacy of $CyaA_{9D2E/9K2R}$ secretion was not enhanced in the presence of 2 mM Ca^{2+} (Figure 6B, central panel). Apart from potentially decreasing the electrophoretic mobility of the RTX block V in the T1SS duct, the charge-reversing substations thus likely interfered also with Ca^{2+}-dependent folding of block V, affecting binding of Ca^{2+} ions by the rest of the RTX domain.

Successive Ca^{2+}-driven folding of RTX blocks at the exit of the T1SS conduit would yield Brownian ratchets and restrict backsliding of the polypeptide chain, while accelerating its forward movement in the T1SS duct. To test this hypothesis, CyaA-specific 3D1 and 9D4 mAb were added to 100 μg/ml into culture media instead of Ca^{2+}. These mAbs recognize different segments of CyaA, the 9D4 recognizing epitopes at the interface of the RTX blocks II and III (data not shown) and the 3D1 binding

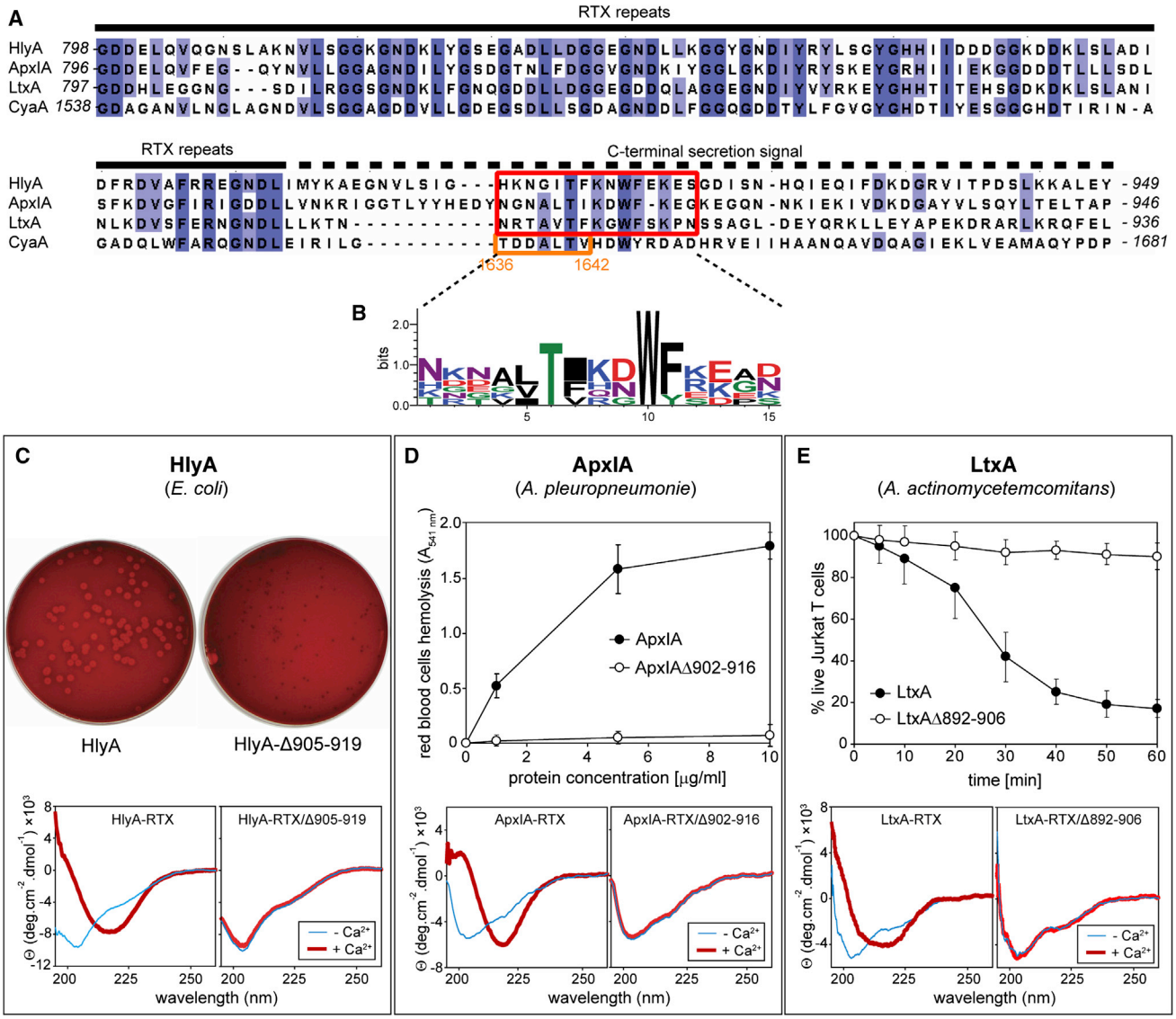

Figure 4. The C-Terminal RTX Folding-Nucleating Capping Structure Scaffold Is Conserved in the RTX Leukotoxin Family

(A) ClustalW2 alignment of the C-terminal sequences of HlyA of *E. coli*, ApxIA of *A. pleuropneumoniae*, LtxA of *A. actinomycetemcomitans*, and CyaA of *B. pertussis*. The degree of conservation is represented by blue color intensity. Residues involved in initiation of Ca^{2+}-induced folding of the RTX domains are indicated by orange and red boxes, respectively.

(B) WebLogo sequence conservation of the motif involved in folding of the C-terminal capping structure of eight RTX leukotoxins (HlyA, ApxIA, ApxII, ApxIII, ApxIVA, LtxA, CyaA, and LktA). The positions are numbered 1 to 15 according to the multisequence alignment provided in (A).

(C) Hemolytic activity of secreted HlyA and HlyA$\Delta_{905\text{-}919}$ on blood agar plates.

(D) Hemolytic activity of purified *A. pleuropneumoniae* ApxIA and ApxIA$\Delta_{902\text{-}916}$ on erythrocytes. The error bars represent ± SD of the mean from at least three independent experiments performed in duplicates.

(E) Cytotoxic activities of recombinant *A. actinomycetemcomitans* LtxA and LtxA$\Delta_{892\text{-}906}$ on Jurkat T cells. The error bars represent ± SD of the mean from at least three independent experiments performed in duplicates. Lower panels in (C), (D), and (E): far-UV CD spectra of HlyA-RTX and HlyA-RTX/$\Delta_{905\text{-}919}$ (C), ApxIA-RTX and ApxIA-RTX/$\Delta_{902\text{-}916}$ (D), and LtxA-RTX and LtxA-RTX/$\Delta_{892\text{-}906}$ (E) in the absence (blue) or presence of 10 mM Ca^{2+} (red lines).

the N-terminal AC segment between residues 373 and 400 (Lee et al., 1999). While the presence of 3D1 mAb had no effect on the basal level of CyaA secretion at 0.1 mM Ca^{2+}, the presence of the RTX-binding 9D4 mAb increased to ~80% the fraction of CyaA molecules that were secreted to cell surface and beyond, causing an ~5-fold enhancement of the AC_{out}/AC_{in} secretion efficacy ratio (Figure 6D, central panel). The increase of the total translocated CyaA amount was also accompanied by a strong enhancement of the release of CyaA into culture supernatants in the presence of 9D4 (Figure 6D, lower panel). Importantly, the 9D4 mAb comparably enhanced also the efficacy of secretion and release of the nonfolding CyaA$\Delta_{1636\text{-}1642}$ protein

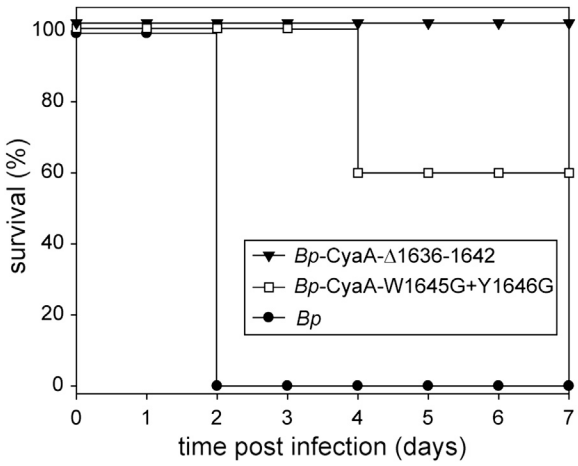

	LD_{50} (CFU per mouse)
Bp	1.0×10^8
Bp-CyaA-Δ1636-1642	N.D. (>1.0×10^{10})
Bp-CyaA-W1645G+Y1646G	1.5×10^9

N.D. (not determined)

Figure 5. Integrity of the C-Terminal Capping Structure Is Required for Folding and Biological Activity of CyaA Secreted by *B. pertussis* during In Vivo Respiratory Infection

Survival of mice after intranasal challenge with wild-type (WT) (*Bp*), *Bp-CyaA*$\Delta_{1636\text{-}1642}$, *and Bp*-CyaA$_{W1645G+Y1646G}$ strains. Animals received 1.5×10^8 CFU of the WT strain and 1.5×10^9 CFU of the *Bp*-CyaA$\Delta_{1636\text{-}1642}$ and *Bp*-CyaA$_{W1645G+Y1646G}$ strains, respectively. The results are means from at least two independent experiments.

(Figure 6D, middle panel). Hence, sequestering of the emerging RTX domain polypeptide into a complex with the 9D4 antibody could in part mimic the Ca^{2+}-dependent Brownian ratcheting and facilitation of forward movement of the CyaA polypeptide through the T1SS duct brought about by folding of the extruded RTX repeats.

DISCUSSION

These data suggest that RTX leukotoxins are equipped with C-terminal capping structures that upon emerging from the T1SS duct undergo Ca^{2+}-triggered folding. The capping structures then scaffold Ca^{2+}-driven folding of the consecutively extruded C-terminal RTX repeat blocks into β-roll assemblies, which act as intramolecular Brownian ratchets that accelerate vectorial translocation of the large RTX polypeptides through the T1SS conduits.

C-terminal RTX repeats are the hallmark of T1SS substrates. Structure similarity search revealed homologs of the overall structure of CyaA$_{1529\text{-}1681}$ segment in the solved structures of T1SS-secreted RTX lipases and proteases (cf. Figure S1). This applied not only to the RTX β-rolls but also to their capping structures. Despite low sequence identity (~10%), these capping segments all exhibit a three-stranded antiparallel β sheet structure, where the distal β strands of the antiparallel β sheet assemblies are positioned parallel to the sequentially penultimate β strands of the β-rolls (cf. Figure S1). Mutagenesis of the capping structures of HlyA, LtxA, and ApxAI then yielded unfolded and inactive toxins (cf. Figure 3).

Determination of structure and analysis of Ca^{2+}-triggered folding dynamics then enabled drawing of the following scenario for the structuring of the C-terminal segment of CyaA upon its extrusion from the T1SS duct. Positioning of carboxyls of Asp_{1609} and Glu_{1654} and of backbone carbonyls of Gly_{1606} and Arg_{1652} would yield formation and loading of the Ca^{2+}(8) binding site. This would yield positioning of the segments of the capping structure and enable a cation-π-π interaction of the side chains of Trp_{1645}, Tyr_{1646}, and Arg_{1624} residues. This would nucleate the assembly of the hydrophobic core and yield positioning of the antiparallel β strand hairpin formed by residues 1,621 and 1,633. Ensuing hydrogen bonding of the antiparallel β strand stack would then enable folding of the entire capping structure and provide C-terminal entropic stabilization for folding of block V into the RTX β-roll (Blenner et al., 2010).

Residues of potentially analogous function as Trp_{1645}, Tyr_{1646}, and Arg_{1624} of CyaA are, indeed, found in the homologous C-terminal sequence motifs of other RTX leukotoxins (cf. Figure 5). Folding of the capping structures of these leukotoxins thus likely involves analogous cation-π-π interactions, involving the aromatic rings of conserved Trp + Tyr or Trp + Phe residue pairs with the guanidinium groups of conserved Arg residues (e.g., Trp_{914}-Phe_{915} in HlyA, Trp_{911}-Phe_{912} of ApxIA, or Trp_{901}-Phe_{902} of LtxA, likely interacting with Arg_{885} of HlyA, Arg_{880} of ApxIA, and Arg_{881} of LtxA, respectively). Indeed, the Trp_{914} residue of HlyA was previously observed to play a role in Ca^{2+}-dependent folding of HlyA (Thomas et al., 2014a), and the activity of HlyA$_{W914A}$ required higher Ca^{2+} concentrations (Sánchez-Magraner et al., 2010), like the activity of CyaA$_{W1645G}$ (cf. Figure 1G).

Remarkably, disruption of the capping structure interfered not only with the Ca^{2+}-driven vectorial folding of the last repeat block of CyaA (150 residues). It impaired also folding of the entire RTX domain. This indicates that the β strand stacking and folding signal propagates from the C-terminal capping structure throughout the five adjacent RTX repeat blocks of the RTX domain. This can now be understood thanks to the SAXS-derived model of RTX domain structure (cf. Figure 3) and with the use of the X-ray structure of block IV–V segment (unpublished data). Both structures indicate that the β-rolls of adjacent RTX blocks are connected by rather rigid β stranded segments that would mediate communication of their hydrophobic cores with the highly hydrophobic core of the C-terminal capping structure. This would yield formation of a contiguous highly hydrophobic interior throughout the entire folded RTX domain. Therefore, once the capping structure has formed and folding of the RTX domain has been triggered by binding of the first Ca^{2+} ion(s), the subsequent binding of further ~35–40 Ca^{2+} ions and the folding of the five consecutive β-rolls of the RTX domain would proceed with high cooperativeness. Indeed, Ca^{2+} titration of the CyaA-RTX domain proceeded as a highly cooperative two-stage process (cf. Figure 2).

The observed vectorial folding of the last RTX repeat block and enhancement of CyaA secretion rate at 2 mM Ca^{2+} allows adding

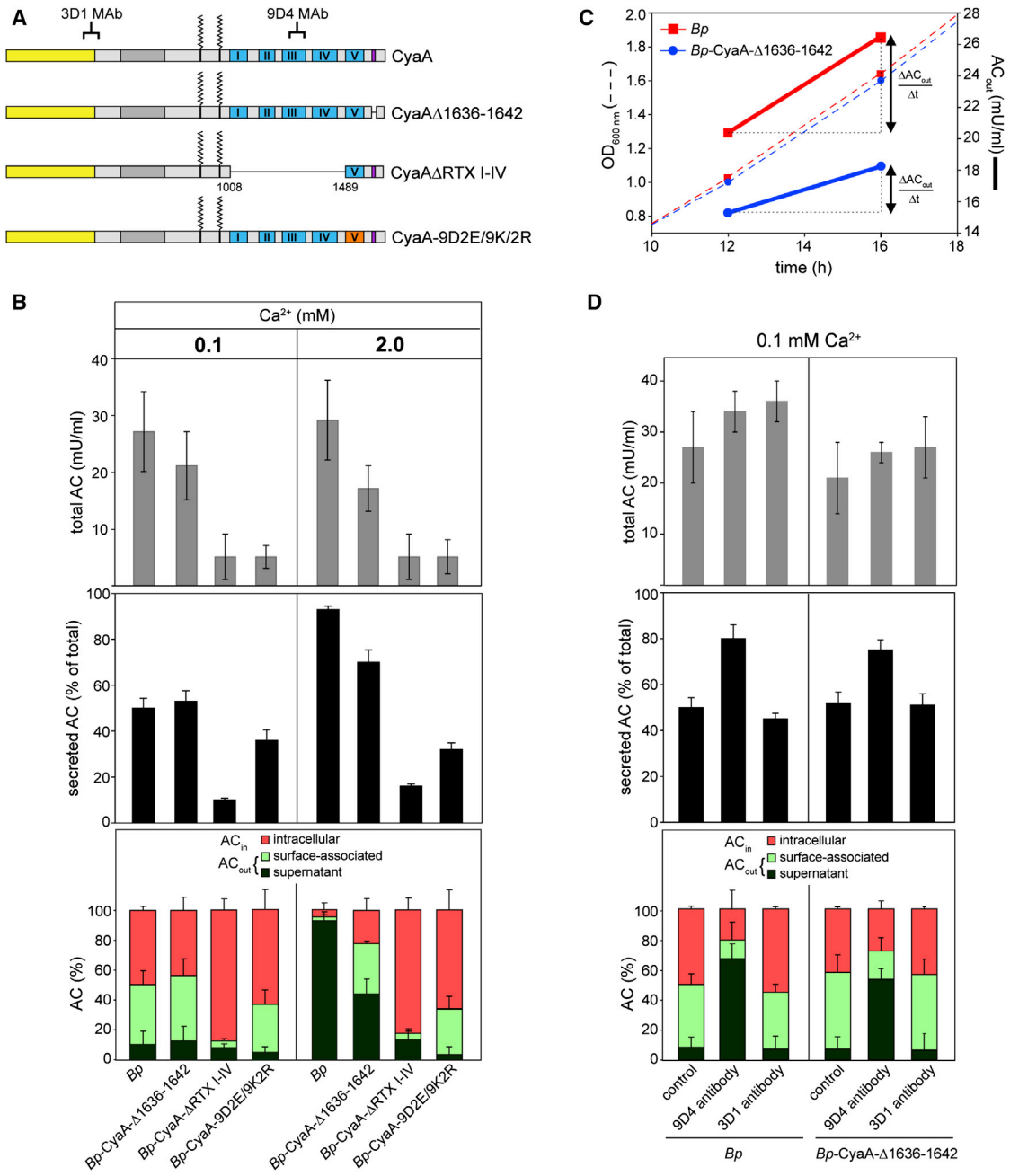

Figure 6. Ca^{2+}-Triggered Folding of RTX Repeat β-Rolls Accelerates CyaA Substrate Translocation through the T1SS Apparatus

(A) CyaA constructs used in secretion experiments. $CyaA_{9D2E/9K2R}$ carries 11 charge-reversing substitutions in the RTX block V, which increases its theoretical isoelectric point (p*I*) from p*I* 3.7 to p*I* 6.6. Location of the 3D1 and 9D4 epitopes is indicated.

(B) T1SS-dependent secretion of intact CyaA and of its RTX domain folding-deficient variants in exponential cultures of *B. pertussis* in media with 0.1 or 2 mM Ca^{2+}. AC enzyme activity was determined in (1) culture supernatants upon addition of urea to a 4 M final concentration, in (2) 4 M urea washes of bacterial cell surface (surface-associated AC), and (3) in 8 M urea extracts of bacterial cells (intracellular AC) prepared once the surface-associated CyaA has been stripped off with 4 M urea. The results are mean ± SD from at least three independent experiments (see Supplemental Information on free Ca^{2+} in SS media).

(C) Secretion kinetics of CyaA (red) and $CyaA\Delta_{1636-1642}$ (blue) proteins at 2 mM Ca^{2+} in two points of exponential growth curve (dotted line). The increase of amount of CyaA secreted per time unit ($AC_{out}/\Delta t$) was 3.6 ± 1.4 pmol.min^{-1} for CyaA and 1.8 ± 1.0 pmol.min^{-1} of $CyaA\Delta_{1636-1642}$.

(D) *B. pertussis* cells were grown at 37°C to OD_{600nm} = 1.0 in SS medium with 0.1 mM Ca^{2+} in the absence or presence of the 9D4 or 3D1 antibodies (100 μg/mL). The results represent mean ± SD from at least three independent experiments.

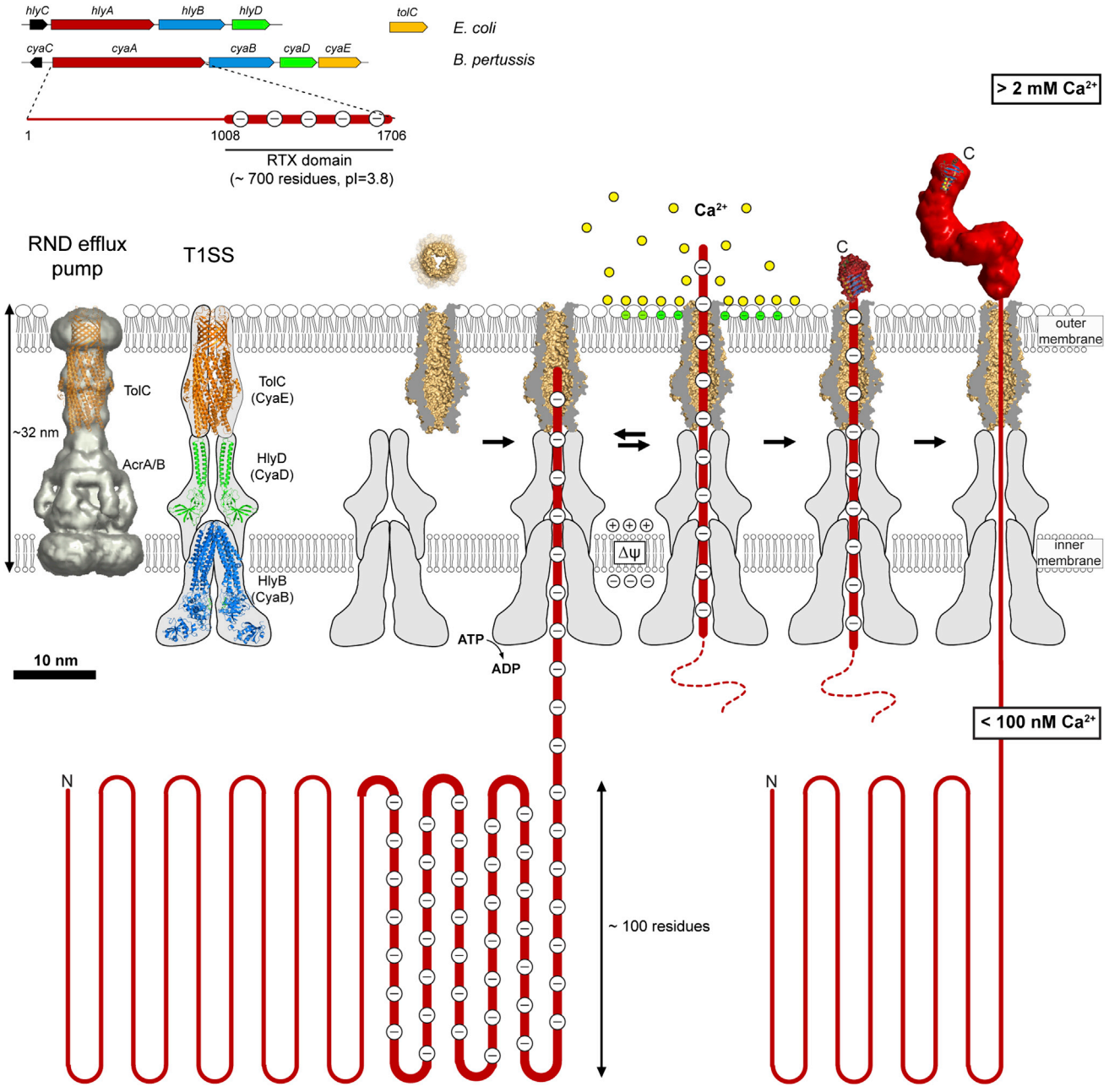

Figure 7. Calcium-Driven Formation of Intramolecular Brownian Ratchets Directs Translocation of RTX Substrates through the T1SS Conduit

Upon engagement of the C-terminal secretion signal by the ATPase component of the T1SS translocator at the cytosolic face of the inner bacterial membrane, a conduit spanning across the entire Gram-negative bacterial cell envelope assembles. The C-terminal end of the unfolded secreted RTX polypeptide interacts with the ABC transporter component of the T1SS assembly and enters the conduit due to action of the ABC ATPase. The proton-motive force represents the negative membrane potential (negative inside/positive outside) that would promote electrophoretic extrusion of the negatively charged RTX polypeptide across the inner membrane portion of T1SS. In the periplasmic section of the conduit, formed by the outer membrane TolC-like homotrimer, the translocating chain may tumble back and forth by Brownian motion. The C-terminal "folding scaffold" is expelled from the outer mouth of the T1SS conduit by electrostatic repulsion from the negatively charged lipid A and KDO-associated phosphate groups and the inner core layer carboxyls of the outer LPS layer.

Outside the conduit, the C-terminal segment of CyaA interacts with Ca^{2+}, and the C-terminal capping structure would then form and enable Ca^{2+}-dependent stacking of the consecutive RTX repeats into a β-roll structure. The thus-formed intramolecular ratchet prevents backsliding of the polypeptide in the T1SS conduit. Folding of successively emerging repeat blocks then increases the magnitude of Brownian fluctuation toward extrusion of the polypeptide from the T1SS opening, thus enhancing efficacy of the ratcheting mechanism and enabling directional extrusion of the very large RTX proteins through T1SS conduits.

(legend continued on next page)

of a push-ratchet mechanism to the current model of T1SS operation (Figure 7). RTX protein translocation through the T1SS duct starts by interaction of the C-terminal secretion signal with the cytoplasmic domain(s) of the ABC transporter (Lecher et al., 2012). A series of events then leads to conformational changes within its transmembrane domain and is followed by reorganization of the periplasmic domain of the MFP component, yielding recruitment of the trimeric OMP component of the T1SS translocator. Assembly of a transenvelope channel-tunnel conduit then induces binding of ATP into the Walker A site of the ABC transporter, yielding opening of the transport pathway entrance of the T1SS channel for insertion of the C-terminal secretion signal of the unstructured RTX substrate. Hydrolysis of ATP provides mechanical energy for conformational changes, generating power strokes that facilitate progressive inserting of the C-terminal RTX repeats into the T1SS conduit. Electrophoretic movement of the negatively charged RTX polypeptide along the gradient of negative membrane potential on the inner (cytoplasmic) bacterial membrane may then facilitate extrusion of the RTX protein from bacterial cytosol across the T1SS duct and may direct it for vectorial movement toward the outer surface opening (Figure 7). Based on reconstructed cryo-electron microscopy map of the homologous TolC/AcrA/B RND efflux complex (Du et al., 2014) and the X-ray structure of TolC (Koronakis et al., 2000), the typical T1SS duct would be ~32 nm in length and would accommodate an unfolded polypeptide of ~100 residues in length. This would translocate through a TolC trimer conduit with an inner cavity of ~16–34 Å in diameter, exiting through a narrow outer opening of only ~10 Å (cf. Figure 7). Ca^{2+} binding then promotes folding of a capping structure that scaffolds the Ca^{2+}-dependent folding of RTX repeats into a β-roll, generating an intramolecular Brownian ratchet that restricts backsliding and accelerates directional extrusion of the polypeptide from the conduit. Cosecretional vectorial folding of consecutively emerging RTX repeat blocks then yields formation of successive Brownian ratchets that accelerate directional movement by restricting back-and-forth tumbling of the RTX substrate in the T1SS duct. This would plausibly be expected to enhance the rate and efficacy of directional movement of particularly large RTX leukotoxins and MARTX polypeptides through the T1SS duct (cf. Figures 6B and 6C).

While ratcheting mechanisms are used also by other protein translocation systems (Matlack et al., 1999; Neupert and Brunner, 2002), the RTX ratchets exhibit several features that make them appear superior. RTX ratchets are formed by an integral part of the translocated polypeptide and thus operate as intramolecular ratchets capable to facilitate secretion without the need for complex chaperone proteins in the extracellular milieu. Further, RTX β barrel ratchets cannot form inside the calcium-depleted bacterial cytosol but form readily outside of the bacterial cell at Ca^{2+} concentrations occurring in plant and animal body fluids.

The experiments at physiological Ca^{2+} concentrations indicate that passive but ratcheted translocation plays an important role in CyaA secretion. Passive transport per se is, however, unlikely to ensure efficient translocation of the often very long RTX polypeptides through the T1SS assemblies. In general, the ABC transporters convert chemical energy of ATP into mechanical energy, controlling early stages of substrate translocation (Davidson et al., 2008), and the action of the ABC transporter component is unlikely to be enough for efficient translocation of larger RTX polypeptides through the T1SS assemblies. Indeed, removal of the four internal blocks of RTX repeats of CyaA ($CyaA\Delta_{RTX\_I\text{-}IV}$) importantly affected secretion of the 1,225-residue-long polypeptide led by a single RTX block, despite an intact capping structure and secretion signal. Hence, the ATPase activity of the T1SS as such and the possible Ca^{2+}-driven folding of the block V outside of the cells were insufficient for translocation of the 1,008-residue-long N-proximal non-RTX portion of CyaA.

Previous work indicated that only the early steps of T1SS-dependent RTX protein secretion would be driven by the electrical potential on the inner bacterial membrane and by the energy derived from ATP hydrolysis by the ABC transporter (Létoffé et al., 1996; Thanabalu et al., 1998). These steps would comprise assembly of the T1SS apparatus, insertion of the C terminus of the RTX substrate into the translocation pathway, and the initial movement of the transported polypeptide within the conduit. Here we show that ~50% of the produced CyaA molecules were still secreted to bacterial surface and beyond it also at low calcium concentrations, at which RTX domain folding outside of bacterial cells did not occur. The ATPase activity of the ABC transporter may thus play a role and operate until the translocation process of large RTX substrates is brought to a point where most of the RTX domain has been extruded from bacterial cytosol. The poor efficacy of $CyaA\Delta_{RTX\_I\text{-}IV}$ secretion would, however, raise the possibility that translocation of RTX substrates may be importantly facilitated by a parallel electrophoretic mechanism, possibly independent of ATP hydrolysis by the ABC subunit of T1SS. Indeed, the removal of a large portion of the highly negatively charged RTX domain importantly impacted the efficacy of CyaA secretion also at low concentrations of Ca^{2+}, where formation of β-roll ratchets did not play a role. The intrinsically disordered RTX domain substrates of T1SS would typically bear a strong negative charge (p*I* ~4) inside the Ca^{2+}-depleted bacterial cytosol. This may enable electrophoretic

The T1SS components were drawn to scale using the reconstructed cryo-electron microscopy map of the homologous TolC/AcrA/B RND efflux complex (EMDB: EMD-5915; Du et al., 2014) and the X-ray structures of TolC (orange, PDB: 1EK9; Koronakis et al., 2000), AcrA (green, PDB: 2F1M; Mikolosko et al., 2006), and of the human mitochondrial ABCB10 ABC transporter (blue, PDB: 4AYT; Shintre et al., 2013), using the NMR structure of C39-like domain of HlyB (PDB: 3ZUA; Lecher et al., 2012). The translocating (linearized) CyaA polypeptides in the lower portion of the figure are also drawn to scale, considering that an unfolded 100-residue-long segment is ~35 nm in length and would span across the entire T1SS assembly conduit of a length of ~32 nm. The RTX domain portion of CyaA is decorated by signs indicating its high negative charge (p*I* 3.8) prior to binding of Ca^{2+}. The negative electrochemical potential ($\Delta\Psi$) on the inner membrane would be one of the energy sources involved in electrophoretic RTX domain translocation across the inner membrane (Koronakis et al., 1991). Negative charges of phosphate groups in the lipid A and inner core of LPS (green balls) would provide electrostatic repulsion of negatively charged RTX chain, contributing to its directional electrophoretic movement through the outer portion of the T1SS conduit.

movement of the RTX polypeptide chain within the T1SS conduit along the negative electrochemical potential across the inner bacterial membrane. It has previously been reported that the total proton motive force was particularly required at an early, but not a late, stage of T1SS-mediated secretion of HlyA (Koronakis et al., 1991). This would go well with our findings that the $CyaA_{9D2E/9K2R}$ construct with much reduced net negative charge of its C-terminal RTX block V was impaired in translocation through the T1SS. Moreover, the efficacy of $CyaA_{9D2E/9K2R}$ secretion was not enhanced in the presence of 2 mM Ca^{2+} (cf. Figure 6C). It thus appears that the charge-decreasing substitutions in $CyaA_{9D2E/9K2R}$ impacted efficacy of an early step of secretion, such as the engagement of the C-terminal segment of $CyaA_{9D2E/9K2R}$ into the translocation apparatus, or its electrophoretic extrusion across the cytoplasmic membrane. It is plausible to propose that secretion of large RTX polypeptides, such as RTX leukotoxins, may thus be energized at least in part by electrophoretic movement of their extensive and highly negatively charged RTX domains through the inner membrane portions of the T1SS assemblies.

EXPERIMENTAL PROCEDURES

Mouse Infection

All animal experiments were approved by the Animal Welfare Committee of the Institute of Microbiology of the ASCR, v.v.i. Handling of the animals was performed according to the Guide for the Care and Use of Laboratory Animals (National Research Council, 2011); the Act of the Czech National Assembly, Collection of Laws No. 149/2004, inclusive of the amendments on the Protection of Animals against Cruelty; and the Public Notice of the Ministry of Agriculture of the Czech Republic, Collection of Laws No. 207/2004, on the care and use of experimental animals.

Molecular Biology

Substitutions in *B. pertussis* CyaA, *E.coli* HlyA, *A. pleuropneumoniae* ApxIA, and *A. actinomycetemcomitans* LtxA were generated in the respective coding sequences by overlap PCR mutagenesis, and all constructs were verified by DNA sequencing.

Protein Production and Purification

Recombinant CyaA and ApxIA proteins were produced as described (Masin et al., 2013). RTX domains of CyaA (CyaA-RTX), ApxIA (ApxIA-RTX), and HlyA (HlyA-RTX) were produced as soluble GST fusions and purified on Ni-NTA beads following TEV processing.

AC Enzyme and CyaA Toxin Activity Determination

Cell binding of CyaA, cAMP accumulation, AC enzyme activity, and hemolysis were determined as described (Bumba et al., 2010; Masin et al., 2013).

Construction of *CyaA* Mutants in *B. pertussis*

Mutated *cyaA* genes were introduced into *B. pertussis* chromosome by allelic exchange (Inatsuka et al., 2010).

Secretion of CyaA by *B. pertussis*

Total CyaA in *B. pertussis* culture fractions was quantified as AC enzyme activity. The efficacy of CyaA secretion (AC_{out}/AC_{in}) was determined as the ratio between the sum (AC_{out}) of the AC activity in the supernatant desorbed with 4 M urea solution from bacterial surface and the intracellular AC activity extracted from the 4 M urea-washed cells with 8 M urea (AC_{in}). All fractions were adjusted to 4 M urea concentration prior to AC enzyme activity assay, and the relative distribution of the AC activities in the three fractions was expressed as percent of total AC activity.

Protein Crystallization and Structure Refinement

Screening of crystallization conditions was performed using a sitting drop vapor diffusion setup using a Gryphon crystallization robot (Art Robbins), together with JCSG core suite I–IV screens (QIAGEN). Diffraction quality $CyaA_{1529-1681}$ crystals were grown in hanging droplets from a 1:1 mixture of the 9 mg/mL protein solution (5 mM Tris-HCl, 150 mM NaCl, 10 mM $CaCl_2$ [pH 7.4]) and the reservoir solution (0.2 M $MgSO_4$, 20% v/v PEG 3350) at 291 K. Diffraction data were collected from a single crystal at 90 K using synchrotron radiation at the MX-14.1 beamline (BESSYII Helmholtz-Zentrum; 0.918 Å) equipped with a Rayonix M-225 CCD camera detector. The structure of $CyaA_{1529-1681}$ was solved by molecular replacement using *PHASER* (McCoy et al., 2007).

Nuclear Magnetic Resonance

Nuclear magnetic resonance (NMR) spectra were recorded at 30°C on 600 MHz and 850 MHz Bruker Avance spectrometers equipped with the triple-resonance $^{1}H/^{13}C/^{15}N$ TCI cryoprobe (Bruker), processed by *NMRPIPE* (Delaglio et al., 1995), and analyzed by using *SPARKY*. The sequential assignment of the resonances was obtained using a standard set of triple resonance experiments. The Ca^{2+}-dependent folding of selected backbone amides was expressed as the relative intensities of the specific crosspeak in the HSQC spectra during calcium titration, where the maximal intensity of the peak was arbitrarily set to 1.

SAXS

The SAXS data were collected using a PILATUS 2M pixel detector (DECTRIS) at the P12 beamline of EMBL (DESY) at a sample-detector distance of 3.1 m and a wavelength of 1.24 Å. Low-resolution ab initio models were calculated using DAMMIF (Franke and Svergun, 2009).

ACCESSION NUMBERS

Structure coordinates have been deposited in the Protein Data Bank under ID codes PDB: 5CVW and 5CXL (http://www.rcsb.org). The assigned backbone resonances (^{1}H, ^{15}N, $^{13}C'$, $^{13}C\alpha$, and $^{13}C\beta$) for $CyaA_{1529-1681}$ have been deposited in the Biological Magnetic Resonance Bank under ID code BMRB: 25863 (http://www.bmrb.wisc.edu). The SAXS models of $CyaA_{1008-1681}$ (RTX domain blocks I to V) and $CyaA_{1529-1681}$ (RTX block V) have been deposited in the Small Angle Scattering Biological Data Bank under ID codes SASDB74 and SASDB84, respectively (http://www.sasbdb.org).

SUPPLEMENTAL INFORMATION

Supplemental Information includes Supplemental Experimental Procedures, seven figures, and two tables and can be found with this article online at http://dx.doi.org/10.1016/j.molcel.2016.03.018.

AUTHOR CONTRIBUTIONS

L. Bumba designed the research, analyzed data, prepared the figures, and wrote the paper; J.M. designed the research and performed the biological assays; P.M. and V.V. performed NMR experiments; T.W. generated mutants; L.M. performed crystallization screening; I.B. carried out qPCR and mice experiments; N.K. performed *B. pertussis* secretion experiments; L. Bednarova carried out CD measurement; M.K. and D.I.S. analyzed the SAXS data; C.B. analyzed the crystallographic data; and P.S. designed the research, interpreted the results, and wrote the paper.

ACKNOWLEDGMENTS

This work was supported by grants 15-11851S, P207/11/0717, 13-14547S, and P302/12/0460 (CSF); GAUK #390213; SVV-2016-260314 (L.M.); and MEYS grants BIOCEV CZ.1.05/1.1.00/02.0109, LK11205, and LO1304. M.K. was supported by Marie Curie grant IDPbyNMR #264257. The X-ray and SAXS data were collected at the MX-14.1 beamline (BESSYII, *Helmholtz-Zentrum Berlin*, *BioStruct-X (N°283570)*) and the P12 beamline of EMBL

(DESY). We thank Jacek Lubkowski for help with structure solving, Jakub Ptacek for screening of crystallization conditions, and Iva Marsikova and Hana Kubinova for technical help. P.S. is founder and shareholder of Revabiotech SE that develops next generation of whole-cell pertussis vaccines. P.S. and J.M. are coinventors on a patent portfolio protecting the use of adenylate cyclase toxin as a pertussis vaccine antigen and antigen delivery tool.

Received: April 27, 2015
Revised: December 31, 2015
Accepted: March 15, 2016
Published: April 7, 2016

REFERENCES

Bauche, C., Chenal, A., Knapp, O., Bodenreider, C., Benz, R., Chaffotte, A., and Ladant, D. (2006). Structural and functional characterization of an essential RTX subdomain of *Bordetella pertussis* adenylate cyclase toxin. J. Biol. Chem. *281*, 16914–16926.

Baumann, U., Wu, S., Flaherty, K.M., and McKay, D.B. (1993). Three-dimensional structure of the alkaline protease of *Pseudomonas aeruginosa*: a two-domain protein with a calcium binding parallel beta roll motif. EMBO J. *12*, 3357–3364.

Bejerano, M., Nisan, I., Ludwig, A., Goebel, W., and Hanski, E. (1999). Characterization of the C-terminal domain essential for toxic activity of adenylate cyclase toxin. Mol. Microbiol. *31*, 381–392.

Blenner, M.A., Shur, O., Szilvay, G.R., Cropek, D.M., and Banta, S. (2010). Calcium-induced folding of a beta roll motif requires C-terminal entropic stabilization. J. Mol. Biol. *400*, 244–256.

Bumba, L., Masin, J., Fiser, R., and Sebo, P. (2010). *Bordetella* adenylate cyclase toxin mobilizes its β2 integrin receptor into lipid rafts to accomplish translocation across target cell membrane in two steps. PLoS Pathog. *6*, e1000901.

Chen, V.B., Arendall, W.B., 3rd, Headd, J.J., Keedy, D.A., Immormino, R.M., Kapral, G.J., Murray, L.W., Richardson, J.S., and Richardson, D.C. (2010). MolProbity: all-atom structure validation for macromolecular crystallography. Acta Crystallogr. D Biol. Crystallogr. *66*, 12–21.

Chenal, A., Karst, J.C., Sotomayor Pérez, A.C., Wozniak, A.K., Baron, B., England, P., and Ladant, D. (2010). Calcium-induced folding and stabilization of the intrinsically disordered RTX domain of the CyaA toxin. Biophys. J. *99*, 3744–3753.

Confer, D.L., and Eaton, J.W. (1982). Phagocyte impotence caused by an invasive bacterial adenylate cyclase. Science *217*, 948–950.

Costa, T.R., Felisberto-Rodrigues, C., Meir, A., Prevost, M.S., Redzej, A., Trokter, M., and Waksman, G. (2015). Secretion systems in Gram-negative bacteria: structural and mechanistic insights. Nat. Rev. Microbiol. *13*, 343–359.

Davidson, A.L., Dassa, E., Orelle, C., and Chen, J. (2008). Structure, function, and evolution of bacterial ATP-binding cassette systems. Microbiol. Mol. Biol. Rev. *72*, 317–364.

Delaglio, F., Grzesiek, S., Vuister, G.W., Zhu, G., Pfeifer, J., and Bax, A. (1995). NMRPipe: a multidimensional spectral processing system based on UNIX pipes. J. Biomol. NMR *6*, 277–293.

Du, D., Wang, Z., James, N.R., Voss, J.E., Klimont, E., Ohene-Agyei, T., Venter, H., Chiu, W., and Luisi, B.F. (2014). Structure of the AcrAB-TolC multidrug efflux pump. Nature *509*, 512–515.

Eby, J.C., Gray, M.C., and Hewlett, E.L. (2014). Cyclic AMP-mediated suppression of neutrophil extracellular trap formation and apoptosis by the *Bordetella pertussis* adenylate cyclase toxin. Infect. Immun. *82*, 5256–5269.

El-Azami-El-Idrissi, M., Bauche, C., Loucka, J., Osicka, R., Sebo, P., Ladant, D., and Leclerc, C. (2003). Interaction of *Bordetella pertussis* adenylate cyclase with CD11b/CD18: Role of toxin acylation and identification of the main integrin interaction domain. J. Biol. Chem. *278*, 38514–38521.

Franke, D., and Svergun, D.I. (2009). DAMMIF, a program for rapid *ab-initio* shape determination in small-angle scattering. J. Appl. Cryst. *42*, 342–346.

Guermonprez, P., Khelef, N., Blouin, E., Rieu, P., Ricciardi-Castagnoli, P., Guiso, N., Ladant, D., and Leclerc, C. (2001). The adenylate cyclase toxin of *Bordetella pertussis* binds to target cells via the αM(β2) integrin (CD11b/CD18). J. Exp. Med. *193*, 1035–1044.

Hewlett, E.L., Gordon, V.M., McCaffery, J.D., Sutherland, W.M., and Gray, M.C. (1989). Adenylate cyclase toxin from *Bordetella pertussis*. Identification and purification of the holotoxin molecule. J. Biol. Chem. *264*, 19379–19384.

Inatsuka, C.S., Xu, Q., Vujkovic-Cvijin, I., Wong, S., Stibitz, S., Miller, J.F., and Cotter, P.A. (2010). Pertactin is required for *Bordetella* species to resist neutrophil-mediated clearance. Infect. Immun. *78*, 2901–2909.

Iwaki, M., Ullmann, A., and Sebo, P. (1995). Identification by in vitro complementation of regions required for cell-invasive activity of *Bordetella pertussis* adenylate cyclase toxin. Mol. Microbiol. *17*, 1015–1024.

Kamanova, J., Kofronova, O., Masin, J., Genth, H., Vojtova, J., Linhartova, I., Benada, O., Just, I., and Sebo, P. (2008). Adenylate cyclase toxin subverts phagocyte function by RhoA inhibition and unproductive ruffling. J. Immunol. *181*, 5587–5597.

Karst, J.C., Sotomayor Pérez, A.C., Guijarro, J.I., Raynal, B., Chenal, A., and Ladant, D. (2010). Calmodulin-induced conformational and hydrodynamic changes in the catalytic domain of *Bordetella pertussis* adenylate cyclase toxin. Biochemistry *49*, 318–328.

Koronakis, V., Hughes, C., and Koronakis, E. (1991). Energetically distinct early and late stages of HlyB/HlyD-dependent secretion across both *Escherichia coli* membranes. EMBO J. *10*, 3263–3272.

Koronakis, V., Sharff, A., Koronakis, E., Luisi, B., and Hughes, C. (2000). Crystal structure of the bacterial membrane protein TolC central to multidrug efflux and protein export. Nature *405*, 914–919.

Lecher, J., Schwarz, C.K., Stoldt, M., Smits, S.H., Willbold, D., and Schmitt, L. (2012). An RTX transporter tethers its unfolded substrate during secretion via a unique N-terminal domain. Structure *20*, 1778–1787.

Lee, S.J., Gray, M.C., Guo, L., Sebo, P., and Hewlett, E.L. (1999). Epitope mapping of monoclonal antibodies against *Bordetella pertussis* adenylate cyclase toxin. Infect. Immun. *67*, 2090–2095.

Lenders, M.H., Weidtkamp-Peters, S., Kleinschrodt, D., Jaeger, K.E., Smits, S.H., and Schmitt, L. (2015). Directionality of substrate translocation of the hemolysin A Type I secretion system. Sci. Rep. *5*, 12470.

Létoffé, S., Delepelaire, P., and Wandersman, C. (1996). Protein secretion in gram-negative bacteria: assembly of the three components of ABC protein-mediated exporters is ordered and promoted by substrate binding. EMBO J. *15*, 5804–5811.

Linhartová, I., Bumba, L., Mašín, J., Basler, M., Osička, R., Kamanová, J., Procházková, K., Adkins, I., Hejnová-Holubová, J., Sadílková, L., et al. (2010). RTX proteins: a highly diverse family secreted by a common mechanism. FEMS Microbiol. Rev. *34*, 1076–1112.

Masin, J., Fiser, R., Linhartova, I., Osicka, R., Bumba, L., Hewlett, E.L., Benz, R., and Sebo, P. (2013). Differences in purinergic amplification of osmotic cell lysis by the pore-forming RTX toxins *Bordetella pertussis* CyaA and *Actinobacillus pleuropneumoniae* ApxIA: the role of pore size. Infect. Immun. *81*, 4571–4582.

Matlack, K.E., Misselwitz, B., Plath, K., and Rapoport, T.A. (1999). BiP acts as a molecular ratchet during posttranslational transport of prepro-alpha factor across the ER membrane. Cell *97*, 553–564.

McCoy, A.J., Grosse-Kunstleve, R.W., Adams, P.D., Winn, M.D., Storoni, L.C., and Read, R.J. (2007). Phaser crystallographic software. J. Appl. Cryst. *40*, 658–674.

Mikolosko, J., Bobyk, K., Zgurskaya, H.I., and Ghosh, P. (2006). Conformational flexibility in the multidrug efflux system protein AcrA. Structure *14*, 577–587.

Neupert, W., and Brunner, M. (2002). The protein import motor of mitochondria. Nat. Rev. Mol. Cell Biol. *3*, 555–565.

O'Brien, D.P., Hernandez, B., Durand, D., Hourdel, V., Sotomayor-Pérez, A.C., Vachette, P., Ghomi, M., Chamot-Rooke, J., Ladant, D., Brier, S., and Chenal, A. (2015). Structural models of intrinsically disordered and calcium-bound folded states of a protein adapted for secretion. Sci. Rep. *5*, 14223.

Sánchez-Magraner, L., Cortajarena, A.L., García-Pacios, M., Arrondo, J.L., Agirre, J., Guérin, D.M., Goñi, F.M., and Ostolaza, H. (2010). Interdomain $Ca^{(2+)}$ effects in *Escherichia coli* alpha-haemolysin: $Ca^{(2+)}$ binding to the C-terminal domain stabilizes both C- and N-terminal domains. Biochim. Biophys. Acta *1798*, 1225–1233.

Satchell, K.J. (2011). Structure and function of MARTX toxins and other large repetitive RTX proteins. Annu. Rev. Microbiol. *65*, 71–90.

Sebo, P., and Ladant, D. (1993). Repeat sequences in the *Bordetella pertussis* adenylate cyclase toxin can be recognized as alternative carboxy-proximal secretion signals by the *Escherichia coli* alpha-haemolysin translocator. Mol. Microbiol. *9*, 999–1009.

Sebo, P., Osicka, R., and Masin, J. (2014). Adenylate cyclase toxin-hemolysin relevance for pertussis vaccines. Expert Rev. Vaccines *13*, 1215–1227.

Shintre, C.A., Pike, A.C., Li, Q., Kim, J.I., Barr, A.J., Goubin, S., Shrestha, L., Yang, J., Berridge, G., Ross, J., et al. (2013). Structures of ABCB10, a human ATP-binding cassette transporter in apo- and nucleotide-bound states. Proc. Natl. Acad. Sci. USA *110*, 9710–9715.

Stainer, D.W., and Scholte, M.J. (1970). A simple chemically defined medium for the production of phase I *Bordetella pertussis*. J. Gen. Microbiol. *63*, 211–220.

Thanabalu, T., Koronakis, E., Hughes, C., and Koronakis, V. (1998). Substrate-induced assembly of a contiguous channel for protein export from *E.coli*: reversible bridging of an inner-membrane translocase to an outer membrane exit pore. EMBO J. *17*, 6487–6496.

Thomas, S., Bakkes, P.J., Smits, S.H., and Schmitt, L. (2014a). Equilibrium folding of pro-HlyA from *Escherichia coli* reveals a stable calcium ion dependent folding intermediate. Biochim. Biophys. Acta *1844*, 1500–1510.

Thomas, S., Holland, I.B., and Schmitt, L. (2014b). The Type 1 secretion pathway - the hemolysin system and beyond. Biochim. Biophys. Acta *1843*, 1629–1641.

Vojtova, J., Kamanova, J., and Sebo, P. (2006). *Bordetella* adenylate cyclase toxin: a swift saboteur of host defense. Curr. Opin. Microbiol. *9*, 69–75.

Welch, R.A. (1991). Pore-forming cytolysins of gram-negative bacteria. Mol. Microbiol. *5*, 521–528.

Zaretzky, F.R., Gray, M.C., and Hewlett, E.L. (2002). Mechanism of association of adenylate cyclase toxin with the surface of *Bordetella pertussis*: a role for toxin-filamentous haemagglutinin interaction. Mol. Microbiol. *45*, 1589–1598.